Propulsion and Power Research 2020;9(1):15–25

http://ppr.buaa.edu.cn/

Propulsion and Power Research

www.sciencedirect.com

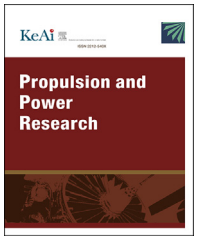

ORIGINAL ARTICLE

Application of laser energy deposition to improve performance for high speed intakes

A. Russell[a,*], M. Myokan[b], H. Bottini[b], A. Sasoh[b], H. Zare-Behtash[a], K. Kontis[a]

[a]*James Watt School of Engineering, University of Glasgow, G12 8QQ, UK*
[b]*Department of Aerospace Engineering, Nagoya University, 464-8603, Japan*

Received 7 August 2018; accepted 15 November 2019
Available online 24 December 2019

KEYWORDS

Laser energy deposition;
Supersonic;
Flow dynamics;
Intakes;
Flow separation

Abstract Research interest has been growing in recent years in supersonic transport, particularly supersonic propulsion systems. A key component of a commonly studied propulsion system, ramjets, is the air intake. For supersonic propulsion systems a major factor in the overall efficiency is the intake pressure recovery. This refers to the ratio of the average total pressure after the intake to that of the freestream. One phenomenon that can have a large effect on this performance index is flow separation at the inlet. The aim of this work is to examine how pulsed laser energy deposition can be used to improve pressure recovery performance by reducing flow separation at the inlet. This research examines the effects of pulsed laser energy deposition upstream of an intake with an axisymmetric centrebody in a Mach 1.92 indraft wind tunnel. Laser frequency was varied between 1 and 60 kHz with an energy per pulse of 5.6 mJ. Schlieren photography was used to examine the fundamental fluid dynamics while total and static pressure downstream of the intake diffuser were measured to examine the resulting effect on the performance. Schlieren imaging shows that the interaction between the laser generated thermal bubble and the leading edge shock produced by the centrebody results in a significant reduction in separation along the intake cone. Analysis of the schlieren results and the pressure results in tandem illustrate that the average separation location along the length of the centrebody directly correlates to the pressure recovery observed in the intake. At the optimal laser

*Corresponding author.
E-mail address: a.russell.2@research.gla.ac.uk (A. Russell).
Peer review under responsibility of Beihang University.

ELSEVIER Production and Hosting by Elsevier on behalf of KeAi

https://doi.org/10.1016/j.jppr.2019.11.002

frequency, found for this Mach number to be 10 kHz, the pressure recovery is found to increase by up to 4.7%. When the laser power added to the system is considered, this results in an overall increase in propulsive power of 2.47%.

Nomenclature

A	cross-sectional area
AR	area ratio
E_{pp}	laser energy per pulse
f	fuel fraction
f_l	laser frequency
M	Mach number
P	static pressure
P_l	laser power
R	ideal gas constant
T	thrust
U	flow velocity

Greek letters

ΔP	net propulsive power increase
γ	gas specific heat ratio
σ	non-dimensional separation location

Subscripts

∞	freestream conditions
e	exit conditions
T	throat conditions
0	stagnation conditions
04	combustion chamber exit conditions

1. Introduction

Supersonic transport is a topic that has seen renewed interest in recent years [1]. A key component that still requires considerable research are supersonic propulsion systems. A key component of an air breathing supersonic propulsion system is the intake and its efficiency. An early type of supersonic intake was the pitot intake which was often a cylindrical channel that used a single normal shock to decelerate the incoming flow. This was improved upon by the addition of a central compression surface upstream of the intake cowl [2]. A major challenge with supersonic intake design is shock boundary layer interaction (SBLI) and boundary layer separation associated with it. Separation at the intake can result in poor performance as a result of lower mass flow ingested (reduces intake compression efficiency) or in the worst cases, unstart.

There have been many attempts to mitigate these effects through flow control, both active and passive. Passive devices are those that cannot have their amplitude modified and cannot be turned on or off. They have advantages in that they are generally cheap, simple devices that are easily installed, an example that is commonly researched in conjunction with supersonic intake design are vortex generators [3,4]. However a problem with passive flow control devices is that they cannot be modulated and the location of influence is fixed. This means that at off-design conditions the benefit they provide will diminish or in some cases have an adverse effect. This is why active flow control devices are often preferred despite their added complexity. A popular example of active flow control applied to supersonic intakes that has been heavily researched is boundary layer suction/bleeding [5−10]. The main issue with boundary layer suction/bleeding is the loss of mass flow rate through the main flow path. An emerging technology for active flow control in high speed flows are energy deposition techniques. These involve adding thermal energy to the flow in a pulsed manner commonly through the means thermal energy [11] of laser energy [12] or plasma actuators [13].

Laser energy deposition is the topic of interest for this research. The fundamental principle is to use high power pulsed laser energy deposition to create thermal bubbles in the flow. These thermal bubbles are a result of rapid energy deposition by the laser [14]. Figure 1 shows step by step the process of laser induced gas breakdown. Breakdown begins when laser energy of large enough power causes multi-photon ionisation of gas molecules. This results in the release of seed electrons that proceed to ionise other gas molecules. This process repeats itself causing a cascading

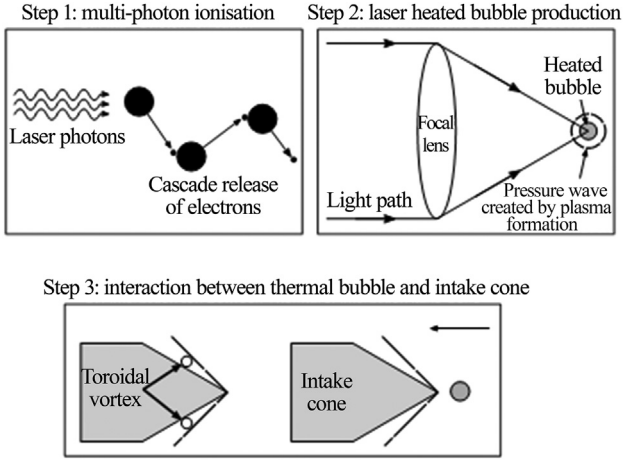

Figure 1 Process of laser induced gas breakdown and interaction with an intake.

release of electrons resulting in plasma formation. The plasma region formed is spherical in this case due to the relatively low static pressure. This hot plasma region results in the release of a blast wave that propagates into the fluid. The thermal bubble created by the plasma is convected downstream as indicated in step 3. It is the interaction between the thermal bubble and the intake cone shock waves that are of interest for this application. The benefit of laser energy deposition as a means of active flow control in comparison to other options include, but are not limited to: the ability to control the input magnitude, the ability to modify the frequency of the input, the ability to change the control location, no loss in intake mass flow rate (this is a significant drawback to boundary layer bleed techniques) and when it is not required it can be turned off and has no negative impact (unlike most if not all passive flow control techniques). Examples of previous applications of laser energy deposition researched include but are not limited to bluff body drag reduction [15,16], control of the Edney IV interaction [17] and control of cavity flows [18]. This research aims to use pulsed laser energy deposition to improve the separation characteristics along an axisymmetric centrebody of a supersonic intake. The separation observed along centrebodies can play a key role in the two well-known variants of buzz that can be experienced by this family of intake known as "big" and "little" buzz [19–21]. The research continues from a fundamental study by Pham et al. [22] on the suppression of resonant instabilities within a supersonic intake using pulsed laser energy deposition. This study will highlight the source of the improvement in pressure recovery of the intake and allow the improvement in overall propulsion system performance, accounting for the addition of laser energy, to be quantified.

2. Experimental details

2.1. Facilities

The facility used was an indraft supersonic wind tunnel with an effective Mach number of 1.92 ± 0.04 for which the static pressure and temperature are 13.8 kPa and 169 K respectively. The static pressure is measured using a transducer mounted in the side wall of the wind tunnel. The total pressure was determined from a measurement of the atmospheric pressure and the assumption that the flow through the wind tunnel nozzle was an isentropic process. The static temperature was also calculated from atmospheric temperature measurements and the isentropic flow assumption made. The laser generated thermal bubbles were created using a repetitive-pulse Nd:YVO_4 laser (wavelength: 1064 nm; capable of pulsing at up to 100 kHz; pulse energy: 5.6 mJ). The laser is directed through a focusing length and through the BK7 window that constitutes one side of the test section to a spot upstream of the model on its central axis. Stable laser induced breakdown was achieved through the experiments up to a deposition frequency of 60 kHz. The power supplied by the laser to the flow is shown for each frequency used in Table 1.

Table 1 Laser power used for each of the pulse frequencies tested.

Laser frequency/Hz	Laser power/W
1	5.6
5	28
10	56
20	112
30	168
40	224
50	280
60	336

Flow visualisation was made available through a laser schlieren setup. The schlieren system was made up from a high speed camera (frame: up to 1280 × 800 pixels; frame rate: up to 8.2×10^6 fps; duration: up to 2048 monochrome 8-bit frames), a laser diode (wavelength: 640 nm; pulse width: 10 ns) two 300 mm diameter concave mirrors and a horizontal knife edge. For this study images were captured at a resolution of 128 × 512 pixels and a frame rate of 130081 fps.

Pressure measurements were also recorded within the test model. Total and static pressures were measured at the ports indicated in Figure 2 using a pressure gauge (TOKYO AIRCRAFT Digital Pressure Gauge DG-920N).

2.2. Test model

The test model in this research has a single angle axisymmetric cone intake and a cowl with a square cross-section. Optical access is available through interchangeable windows on either side of the cowl. The centrebody is a 15° half apex angle cone, 14 mm in length (length that protrudes from the cowl) and 11 mm in diameter. The cowl of the intake is 19 mm × 19 mm internally and is 149 mm long. This results in an intake with an equivalent hydraulic diameter (to that of an intake with a circular cowl) of 19 mm. This would result in a contraction ratio of 2.98. The plug at the rear of the intake model can be moved in either

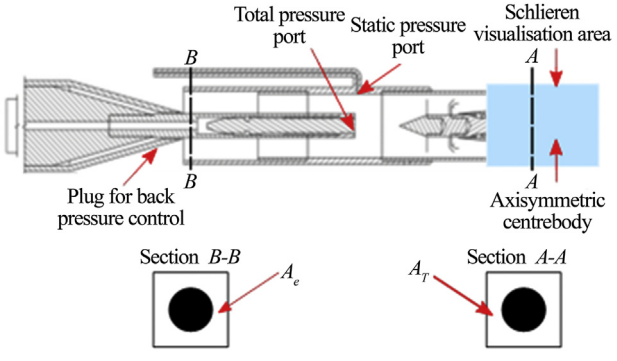

Figure 2 Intake model schematic.

direction by a screw and is the means to control the back pressure experienced by the intake. The area ratio, $AR = \frac{A_T}{A_e}$, defines the measure of back pressure where A_T is the cross-sectional area of the flow path at the exit of the model intake and A_e is the cross-sectional area of the flow path at the entrance to the intake (a visualisation of this is shown in Figure 2). The larger the value of AR, the greater the value of the back pressure experienced by the intake.

3. Schlieren visualisation

As discussed previously, high speed schlieren photography was used to visualise the flow features in this configuration. Figure 3 shows a series of individual schlieren images that allow certain key flow features to be observed. Each feature is a result, at different times in the cycle, of a single laser heated bubble pulse. At time 0 μs the high temperature bubble can be seen in the top right of the image immediately before it reaches the centrebody. This image provides a good representation of the baseline flow field for the intake geometry examined. The normal shock highlighted indicates that the intake is operating in the subcritical mode. Figure 4 provides an illustration of the key features observed when an intake is operating in this mode of operation. The fundamental flow is driven by a pressure within the intake that cannot be supported by an internal shock system. Therefore a normal shock is observed on the external compression surface which decelerates the flow to subsonic speeds as it enters the isolator. The reduced mass flow rate in this operating mode results in significant spillage around the outside of the intake. This expected mass flow spillage is also clearly visible in the first schlieren image. The expected flow separation downstream of the intake is one of the features associated with intake "buzz", mentioned in the introduction.

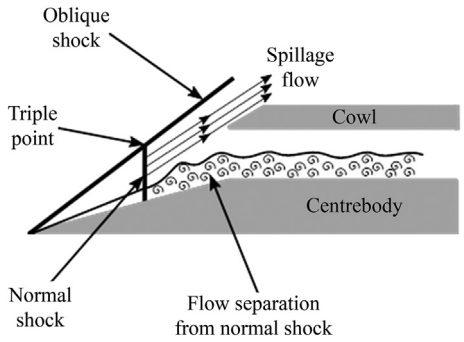

Figure 4 Illustration of the key features associated with an inlet operating in the subcritical mode.

One frame later, at 7.69 μs, the bubble has reached the centrebody and has formed a torus, wrapped around the centrebody. At 30.75 μs there is already evidence of separation on the centrebody being suppressed, by 130.69 μs the

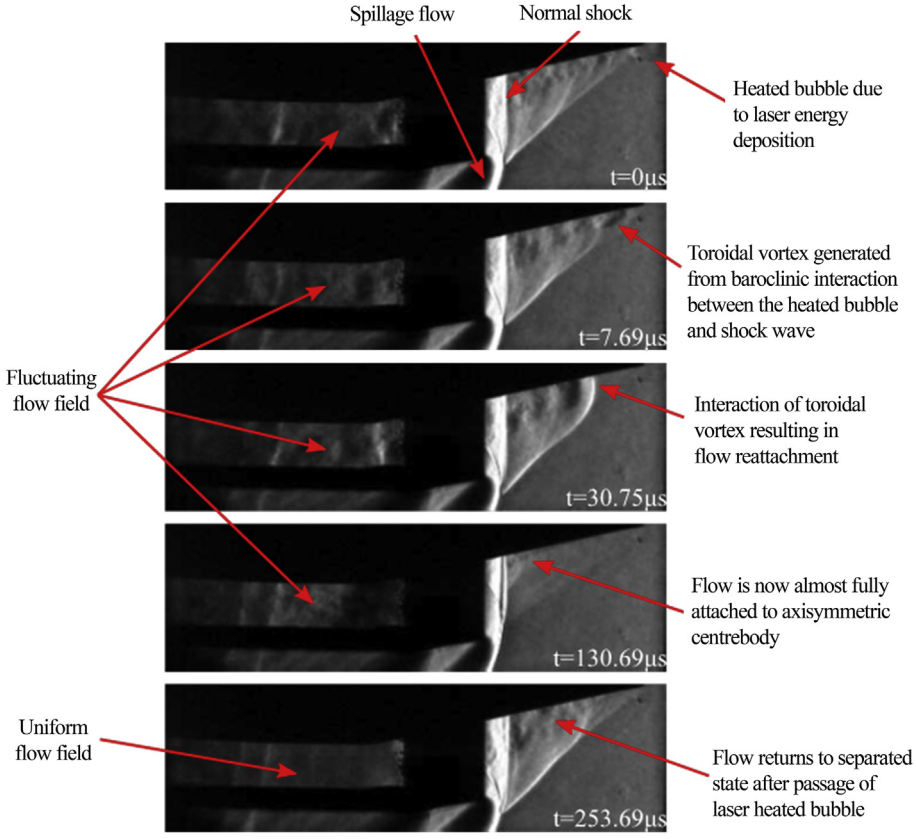

Figure 3 Schlieren images of key points in cycle of interaction between laser heated bubble and centrebody flow field.

flow is attached along almost the entire length of the centrebody. The reattachment is thought to be due to the vorticity generated through the baroclinic instability due to the interaction between the thermal bubble and the shock wave at the tip of the centrebody. Baroclinicity is a term used to describe a misalignment of the pressure and density gradients. This misalignment generates vorticity, mathematically represented by the cross product of the two vectors. Figure 5 illustrates the two vectors in question and their orientation relative to each other.

The Reynolds number at the axisymmetric centrebody is in the region of 1.8×10^5 which suggests a laminar boundary layer (assuming a transition point near a Reynolds number of 5×10^5 [23]). Therefore without the laser energy deposition this laminar boundary layer would be liable to separate due to the adverse pressure gradient, as is clear from the baseline case. However the vorticity produced due to the baroclinic interaction is thought to promote transition from a laminar to a turbulent boundary, making it more resistant to separation as a result of the adverse pressure gradient [12]. It is this phenomenon that is believed to be the reason for the visible changes in the flow field as discussed below. Another interesting feature observed is the apparent reduction in flow unsteadiness observed in the isolator as the toroidal vortex passes through the intake. This is characterised by the distinct variations in intensity in the images from 0 to 130.68 μs followed by the much more uniform image intensity in the final image at 253.69 μs.

From image to image, in some cases, the impact of the laser bubble on the flow features is not immediately clear. To aid visualisation of these effects, image processing was carried out on the raw schlieren images. Each image was subtracted from the mean image and the absolute value of each pixel was taken, resulting in an image illustrating the absolute deviation from mean. Although the actual values of the grayscale in these images have no physical quantity related to them, what they do show is an indication of areas with changing density gradients. Areas that are brighter in the images will, generally, illustrate areas of unsteadiness in the flow. Figures 6 and 7 show a series of these absolute deviation from mean images for no laser pulses and 1 kHz, 10 kHz, and 30 kHz frequency of laser energy deposition. Figure 6 shows the no laser pulse and 1 kHz pulsed laser deposition image series. At a glance, it can be observed that the series with no laser pulses (left) is largely the same from image to image as there is no significant change from one image to another. The separated region is show by the area along the length of the intake cone that has region of intensity greater than 0 (black areas) as here the flow is unsteady and will have a non-negligible standard deviation. However if the 1 kHz series is examined it is evident that the laser pulse has a large effect on the separation characteristics along the length of the cone. There are sections of the time series highlighted for the 1 kHz case: **A** refers to the time over which the flow is reattaching along the length of the centrebody, **B** refers to the period of time over which the flow is almost fully attached and **C** is the period of time that attached flow appears within the diffuser. The areas outlined by the red polygons in section B highlight the areas that have close to 0 standard deviation. This indicates that the flow in these areas is no longer separated in comparison to the no pulsed laser case. Now if the 1 kHz case is compared to the 10 kHz laser frequency (Figure 7), regions of attached flow can still be observed but are shorter. This trend continues with the 30 kHz laser frequency case (Figure 7) to the point where there are no obvious regions of attached flow visible in the diffuser. Due to the highly frequency of the pulsing for the 30 kHz case there is very little oscillation actually observed. The intensity observed in this image is merely noise and is not indicative of any oscillatory behaviour as is more prevalent with the 1 kHz and 10 kHz cases. In general, these deviation from mean images are less helpful at higher frequencies as the noise content becomes significant in comparison to the flow features of interest. They do however provide useful insight into the cycle of behaviour shown for the 1 kHz and for, to a lesser extent, the 10 kHz case.

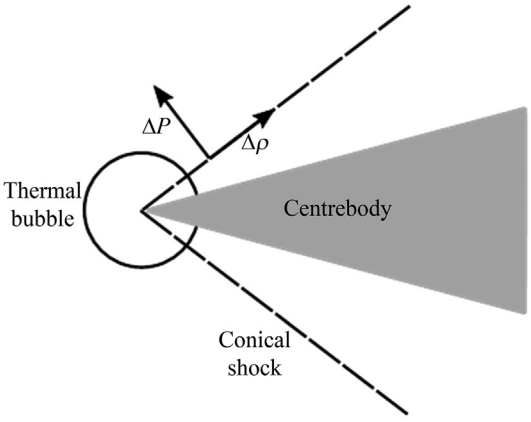

Figure 5 Illustration of the relative orientations of the density gradient associated with the laser generated thermal.

This trend can be further highlighted if quantitative data is extracted from the schlieren images. It is possible to extract separation location along the centrebody through careful examination of the raw images. This was done by tracking the separation point along the centrebody using the raw schlieren images. The time history of the flow separation point on the centrebody is presented in Figure 8. ψ, on the vertical axis, refers to the distance from the tip of the centrebody in the streamwise direction non-dimensionalised by the total length of the centrebody. The trends in separation location agree with what was observable at a glance from the individual schlieren images. For a laser frequency of 1 kHz there is an obvious spike from approximately 0.9 to 1.0 ms in which the flow is almost fully attached. However other than the single spike the location of separation is broadly the same as that of the baseline case (no laser). At 10 kHz laser frequency, individual spikes are still visible in the time history as with the 1 kHz case, but the separation point does not decay back to the baseline

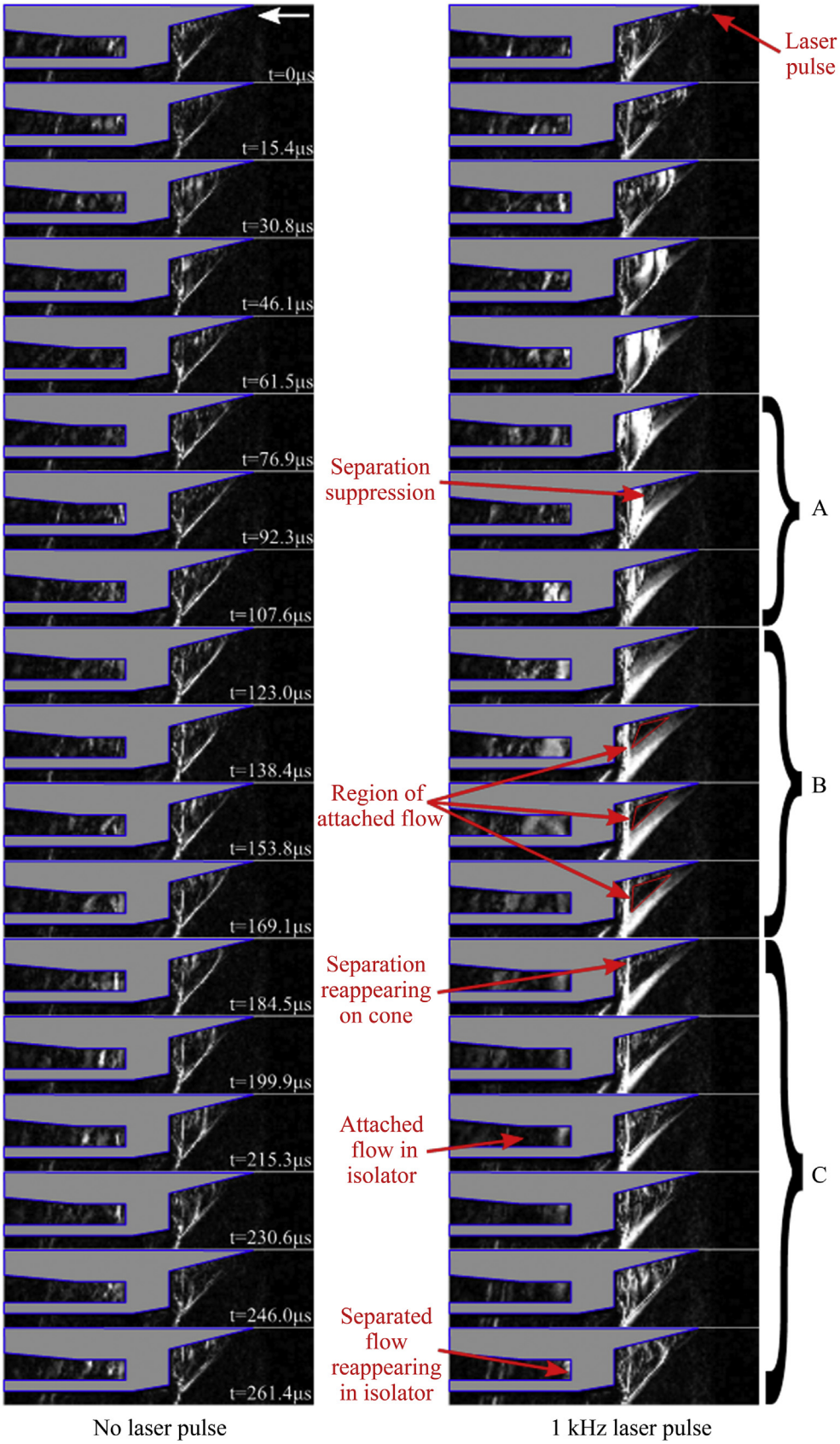

Figure 6 Time series of absolute instantaneous deviation from mean schlieren images for baseline (no laser) and 1 kHz.

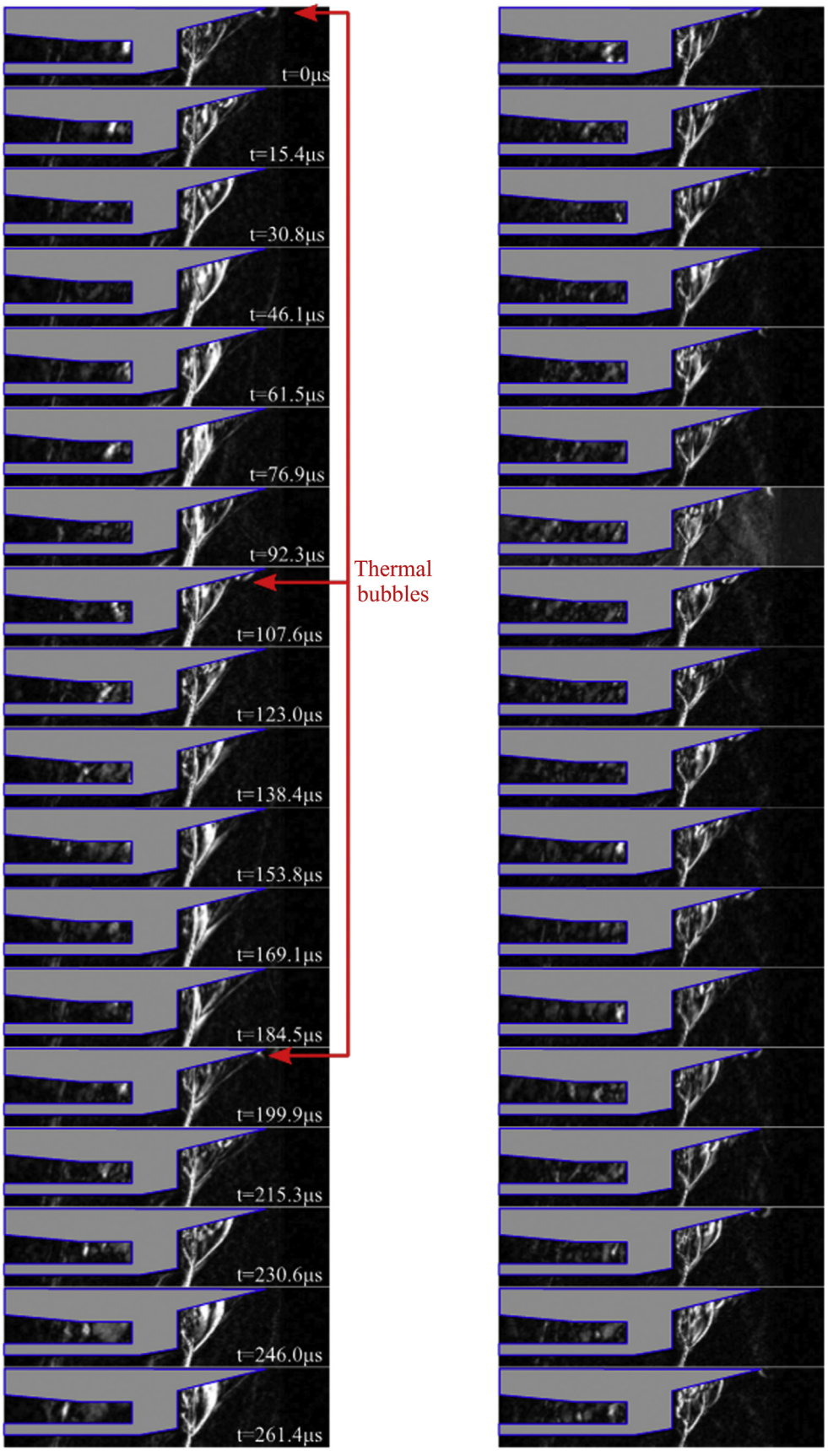

Figure 7 Time series of absolute instantaneous deviation from mean schlieren images for 10 kHz and 30 kHz laser.

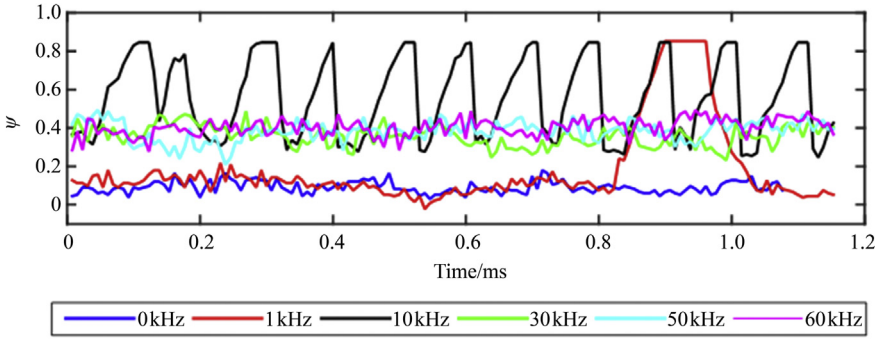

Figure 8 Variation of non-dimensionalised separation location (ψ) with time for a range of laser energy deposition.

separation location as is the case for 1 kHz. It is thought that this is due to the next energy pulse reaching the centrebody before the full cycle could be completed. For the 30, 50 and 60 kHz laser frequency cases the separation location does not show any distinct spikes. For all of these cases there appears to be an offset applied to the baseline case, moving the separation location along the centrebody. The reason that these cases do not show similar responses to the 1 kHz and 10 kHz laser frequency cases is thought to be due to the interference between consecutive pulses. Due to the constant Mach number of the flow, as the laser frequency increases, the time between laser pulses interacting with the centrebody decreases. It would appear that, for the frequencies tested, 10 kHz is the optimal frequency to maximise the length of the attached flow on the centrebody without consecutive laser pulses negatively interfering with each other.

This is shown clearly in Figure 9 as 10 kHz has the largest average value for ψ. It also indicates the plateau that is reached at the higher frequencies of 30 kHz, 50 kHz and 60 kHz. This trend matches data acquired regarding pressure measurements in a previous study [22]. Figure 10 shows average total and static pressure recovery percentages. Here, ΔP is the percentage change in pressure (total and static) relative to the baseline case. The measurement locations and methods for these quantities are described in an earlier section.

It is immediately apparent that the trend in separation location is mirrored in the pressure data, particularly the total pressure. The improvement in total and static pressure recovery in the diffuser is thought to be linked to the scale of the separated region entering the isolator. The further along the centrebody that the flow travels before separating, the less the separated layer will grow by the time it reaches the isolator inlet. This results in a larger proportion of the flow being a separated flow. Flow separation is well known to reduce total pressure recovery [24] and as such this is assumed to be the reason for the improved intake performance associated with the pulsed laser energy deposition. The authors believe that the primary factor resulting in 10 kHz providing the optimal results is the freestream velocity. As shown previously the total pressure recovery relates directly to the length of the centrebody flow that has attached flow. From the time history of the separation location it is clear that beyond a specific frequency the cyclic nature of the separation location disappears. Beyond this frequency it is believed that consecutive heated bubbles interact with each other, breaking down this cycle. The limiting frequency when consecutive bubbles begin to interact with one another would increase if the freestream velocity increased.

4. Effect of pressure recovery on propulsion system performance

It is evident in Figure 10 that the laser energy deposition has a measurable effect on the efficiency of pressure recovery within the intake. However what has not been

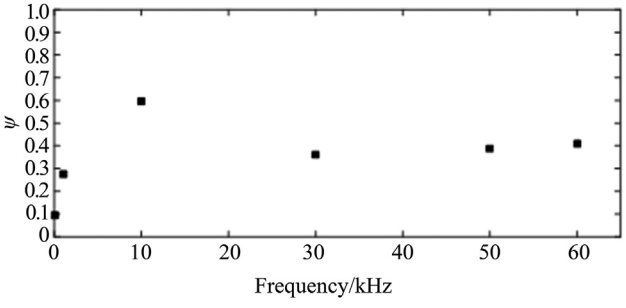

Figure 9 RMS of the non-dimensionalised separation location (ψ).

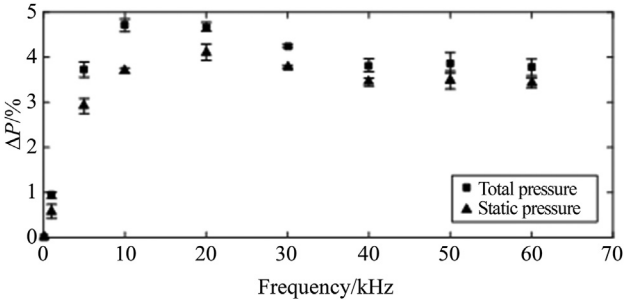

Figure 10 Effect on pressure recovery of upstream laser energy deposition.

examined thus far is how this change affects the performance of the propulsion system. To provide an insight into the potential impact on performance, a hypothetical ramjet engine is considered and the impact of a change in total pressure recovery taken into account.

To begin, a number of key assumptions/statements regarding this theoretical ramjet should be highlighted:

- The nozzle is designed to expand to ambient pressure for the baseline design (no laser energy).
- The expansion in the nozzle is isentropic.
- The exit of the combustor is choked under the standard operating condition.
- The flow throw the combustor can be considered an example of a Rayleigh flow (non-adiabatic flow through a constant area duct with heat addition). This is a somewhat unrealistic assumption and will predict a higher fuel flow rate than reality, however it is a reasonable assumption for the purposes of this analysis.
- The spillage drag does not vary with laser energy deposition (appears to be a reasonable assumption based on the schlieren imaging).
- The combustor experiences 100% efficiency for fuel burn (in reality not the case but as the interest here is the difference in two examples where the same assumption is considered, it is assumed to have little impact).

From these assumptions the following calculation process can be followed. The Mach number at the combustor entrance can be calculated from the total and static pressure measurements along with the standard relationship for stagnation pressure ratio, Eq. (1):

$$\frac{P_0}{P_s} = \left(1 + \frac{\gamma - 1}{2} M^2\right)^{\frac{\gamma-1}{\gamma}} \tag{1}$$

This equation can be rearranged and solved for Mach number. From the Rayleigh flow assumption made regarding the flow through the combustor, and due to the assumption that the design point is for a choked flow at the exit of the combustor; the stagnation temperature ratio across the combustor can now be calculated using Eq. (2):

$$\frac{T_{05}}{T_{04}} = \left(\frac{1 + \frac{\gamma-1}{2} M_5^2}{1 + \frac{\gamma-1}{2} M_4^2}\right) \left(\frac{M_5^2}{M_4^2}\right)^2 \left(\frac{1 + \gamma M_4^2}{1 + \gamma M_5^2}\right) \tag{2}$$

where subscript “04”and “05” represents stagnation properties at the combustor entrance exit respectively. The increase in stagnation temperature calculated is a direct result of the combustion of fuel that occurs within the isolator, the flow fraction of which can be calculated from Eq. (3):

$$f = \frac{C_p(T_{05} - T_{04})}{\Delta H} \tag{3}$$

where f is the fuel flow fraction, C_p is the specific heat capacity of the gas and ΔH is the enthalpy of combustion of the fuel (assumed to be hydrogen for this example). The mass flow rate entering the combustor can also be calculated using Eq. (4):

$$\dot{m}_4 = \frac{\gamma}{\left(\frac{\gamma+1}{2}\right)^{\frac{\gamma+1}{2(\gamma-1)}}} \left(\frac{P_{04} A_4}{\sqrt{\gamma R T_{04}}}\right) \frac{A^*}{A_4} \tag{4}$$

The product of $\dot{m}_4$ and f gives the dimensional fuel mass flow rate. Figure 11 presents the variation, relative to the baseline case, in fuel mass flow rate as a percentage change. This represents a reduction in up to 3.7% of fuel mass flow rate at the optimal laser frequency, 10 kHz.

However another consideration alongside this is how this change affects the thrust produced by the ramjet at this operating condition. In order to determine this, the outlet condition of the nozzle has to be calculated for each condition. As stated in the assumptions, this particular case examined assumes that the baseline ramjet, with a choked flow at the combustor exit/nozzle inlet expands to ambient

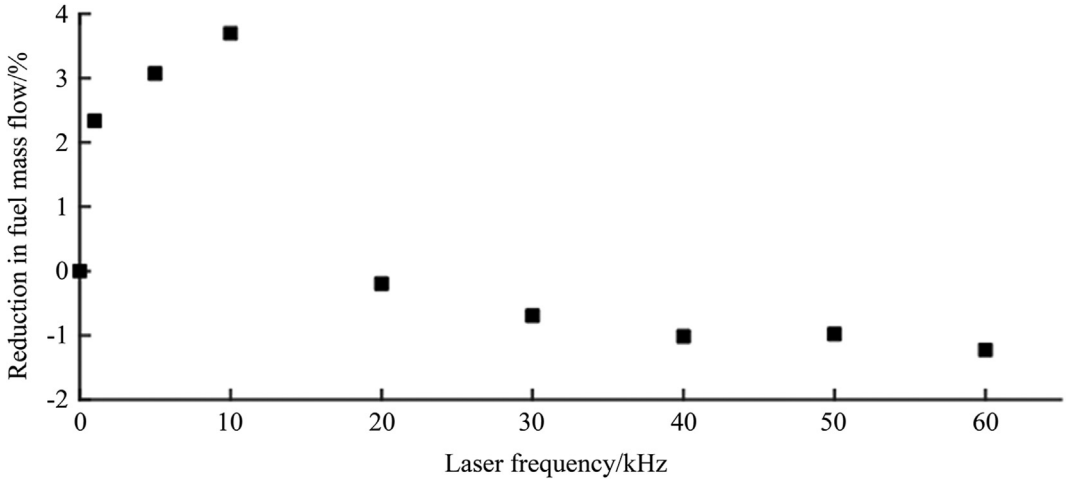

Figure 11 Effect on fuel flow rate of laser pulse frequency.

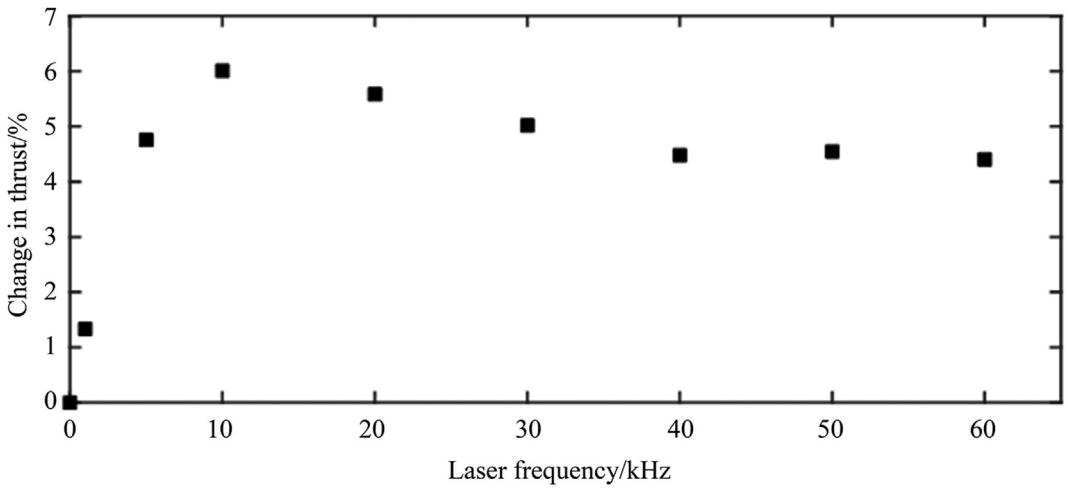

Figure 12 Effect on potential engine thrust of pulsed laser energy deposition.

pressure. This means that the nozzle is sized based on the pressure condition downstream of the combustor at the baseline, no laser energy deposition, condition. However, due to the improved pressure recovery for the pulsed laser energy cases, the total pressure at the combustor exit/nozzle inlet is not consistent between all of the cases. Therefore the exit pressure at the nozzle will vary for each case.

The initial nozzle can be sized based on the isentropic assumption and the calculated stagnation pressure at stage 5. This results in an area ratio between the nozzle inlet and the nozzle exit (assuming a choked flow at the nozzle inlet) of $\frac{A_6}{A_5} = \frac{A_6}{A^*} = 1.207$. This is assuming that the nozzle expands to the static pressure of the freestream. For this area ratio, the exit static pressure can be calculated for each of the other cases (those with pulsed laser energy deposition) using the isentropic relationship.

Based on the assumptions stated earlier regarding spillage drag being equal in all cases the change in thrust relative to the baseline case can be calculated using Eq. (5):

$$\Delta F = [\dot{m}_6 V_6 - \dot{m}_0 V_\infty + (P_6 - P_\infty)A_6]_{Laser} - [\dot{m}_6 V_6 - \dot{m}_0 V_\infty + (P_6 - P_\infty)A_6]_{Baseline} \quad (5)$$

and as the mass flow rate, freestream velocity and pressure at the entrance to the inlet are assumed to be the same for every case (due to assumption that mass flow rate of the spillage flow does not change between cases) this can be simplified down to Eq. (6):

$$\Delta F = [\dot{m}_6 V_6 + P_6 A_6]_{Laser} - [\dot{m}_6 V_6 + P_6 A_6]_{Baseline} \quad (6)$$

Figure 12 illustrates how the change in performance would impact thrust. This percentage change in thrust is based on ΔF calculated in Eq. (6) divided by the thrust of the baseline engine. The baseline engine thrust is calculated assuming no spillage drag. This is not physical however as these calculations are simply to provide an example of the potential impact of the laser energy deposition. The neglect of the spillage drag is not thought to have a significant impact on the results however, as it has not been measured, it must be considered as an uncertainty within this analysis. These calculations suggest that the thrust increases following the same trend as the total pressure recovery. This is sensible as, for the specific case examined here, the rise in total pressure within the intake results in an increase in exit static pressure at the nozzle. This will result in an increase in thrust based on Eq. (6).

This is one very specific example of the impact that this technique could have on a hypothetical engine, however there are many parameters that are unknown or assumed. It is also not clear how heat addition from the combustor may impact the performance. The back pressure generated by a combustor is approximated here by the plug within the intake model that can be moved to alter the back pressure experienced by the intake. The impact of scaling this control method to a larger model has also not been examined. Yet, while this is an isolated example, it does suggest that there is potential for this technique to provide significant benefits to the performance of a ramjet. There is scope for significant further research into more scenarios, intake geometries, freestream speeds etc. and how the laser energy deposition effect changes with these parameters.

5. Conclusions

The aim of this study was to investigate the effect of laser energy deposition on the fluid dynamics environment for a supersonic single angle axisymmetric cone intake. Through careful examination of schlieren imaging it was possible to pseudo-quantitatively measure separation location along the length of the axisymmetric centrebody. The data showed that laser energy deposition could be used to reduce separation.

Examination of the schlieren images suggested that this optimal value is a function of the laser heated bubble

convection velocity (determined by the wind tunnel operating speed and hence freestream Mach number). This is a result of consecutive laser heated bubbles interacting with one another at higher laser frequencies. It is believed that with further studies an empirical relationship could be generated to relate flow velocity to pressure recovery improvement.

The pressure recovery data recorded shows a definitive performance improvement of the intake. When the pressure recovery was used as an input for a hypothetical propulsion system, laser energy deposition was shown to improve fuel consumption by up to 3.7% for the same combustor operating condition. Due to the number of assumptions made in the analysis carried out, these results are speculative and would require further study in order to give accurate values. However, this study suggests that using laser energy deposition to improve the performance of a supersonic propulsion system as a unit or, more specifically, a supersonic intake is a promising opportunity. With further research and optimisation, alongside improvements in laser technology, it may be possible to improve the performance benefits observed in this study even further.

To further investigate this work it would be prudent to test this hypothesis by conducting the same experiment at a range of Mach numbers to confirm that the optimal frequency for improved pressure recovery is dependent on flow velocity. It would also be interesting to record pressure data (using either transducers on a scaled up model or pressure sensitive paint) along the centrebody so as to achieve a better measure of the separation location. Finally it would be useful to gather phase locked total pressure recovery and schlieren/pressure data to measure separation location so that the fundamental relationship between separation location and pressure recovery could be better understood.

Acknowledgements

The authors are grateful to the various staff at Nagoya University. The funding provided by the University of Glasgow via the School of Engineering Mobility Scholarship was also essential in allowing this research to take place.

References

[1] C. Nelson, H.R. Welge, J. Bonnet, Supersonic vehicle systems for the 2020 to 2035 timeframe, in: 28th AIAA Applied Aerodynamics Conference, 2010.

[2] K. Oswatitsch, Pressure recovery for missiles with reaction propulsion at high supersonic speeds (The efficiency of shock diffusers), NACA-TM-1140, 1947.

[3] H. Babinsky, Y. Li, C.W. Pitt Ford, B. Anderson, J. Edwards, J. Debonis, J. Mace, Microramp control of supersonic oblique shock-wave/boundary-layer interactions, AIAA J. 47 (3) (2009) 668−675.

[4] A. Valdivia, K.B. Yuceil, J.L. Wagner, N.T. Clemens, D.S. Dolling, Control of supersonic inlet-isolator unstart using active and passive vortex generators, AIAA J. 52 (6) (2014) 1207−1218.

[5] G.A. Mitchell, R.C. Campbell, Performance of a supersonic ramp-type side inlet with ramp-scoop throat and varying fuselage boundary-layer removal Mach number range 1.5 to 2.0, NACA-RM-E56I26, 1957.

[6] L.J. Obery, R.W. Cubbison, Effectiveness of boundary-layer removal near throat of ramp-type side inlet and free-stream Mach number of 2.0, NACA-RM-E54I14, 1954.

[7] P.C. Simon, Performance of a double-ramp side inlet with combinations of fuselage, ramp, and throat boundary-layer removal, Mach number range, 1.5 to 2.0, NACA-RM-E56G09A, 1956.

[8] R.C. Campbell, Performance of supersonic ram-type side inlet with combinations of fuselage and inlet throat boundary-layer removal, NACA-RM-E56A17, 1960.

[9] B.W. Sanders, R.W. Cubbison, Effect of bleed-system back pressure and porous area on the performance of an axisymmetric mixed compression inlet at Mach 2.5, NASA TM X-1710, 1968.

[10] M.R. Soltani, J.S. Younsi, M. Farahani, Effects of boundary-layer bleed parameters on supersonic intake performance, J. Propuls. Power 31 (3) (2015) 826−836.

[11] L. Yang, E. Erdem, K. Kontis, Flow control using thermal bumps in hypersonic flows, in: 48th AIAA Aerospace Sciences Meeting Including the New Horizons Forum and Aerospace Exposition, 4-7 January 2010.

[12] T. Osuka, E. Erdem, N. Hasegawa, R. Majima, T. Tamba, S. Yokota, A. Sasoh, K. Kontis, Laser energy deposition effectiveness on shock-wave boundary-layer interactions over cylinder-flare combinations, Phys. Fluids 26 (9) (2014) 096103.

[13] S. Im, H. Do, M.A. Cappelli, Plasma control of an unstarting supersonic flow, in: 17th AIAA International Space Planes and Hypersonic Systems and Technologies Conference, 2011.

[14] A. Russell, H. Zare-Behtash, K. Kontis, Joule heating flow control methods for high-speed flows, J. Electrost. 80 (2016) 34−68.

[15] A. Sasoh, Y. Sekiya, T. Sakai, J. Kim, A. Matsuda, Supersonic drag reduction with repetitive laser pulses through a blunt body, AIAA J. 48 (12) (2010) 2811−2817.

[16] A. Sasoh, J.H. Kim, K. Yamashita, T. Sakai, Supersonic aerodynamic performance of truncated cones with repetitive laser pulse energy depositions, Shock Waves 24 (1) (2014) 59−67.

[17] R.G. Adelgren, H. Yan, G.S. Elliot, D.D. Knight, T.J. Beutner, A.A. Zheltovodov, Control of Edney VI interaction by pulsed laser energy deposition, AIAA J. 43 (2) (2005) 256−269.

[18] I. Yilmaz, S. Aradag, An assessment of the effects of laser energy deposition for cavity flows, Int. J. Mach. Mach. Mater. 1 (2) (2013) 158−161.

[19] A. Ferri, L.M. Nucci, The origin of aerodynamics instability of supersonic inlets at subcritical conditions, NACA-RM-L50K30, 1951.

[20] C.L. Dailey, Supersonic diffuser instability, PhD Thesis, California Institute of Technology, 1954.

[21] P. Duveau, S. Trappier, S. Deck, Experimental study of supersonic inlet buzz, AIAA J. 44 (10) (2006) 2354−2365.

[22] M. Myokan, T. Tamba, A. Iwakawa, H.S. Pham, A. Sasoh, Effects of repetitive laser energy deposition on supersonic duct flows, AIAA J. 56 (2) (2017) 1−12.

[23] D.P. De Witt, Fundamentals of Heat and Mass Transfer, third ed., Wiley, 1990.

[24] M.R. Soltani, J.S. Younsi, A. Daliri, Performance investigation of a supersonic air intake in the presence of the boundary layer suction, Proc. Inst. Mech. Eng. G J. Aerosp. Eng. 229 (8) (2015) 1495−1509.